

# **IEICE** **TRANSACTIONS**

## **on Communications**

**VOL. E101-B NO. 2**  
**FEBRUARY 2018**

**The usage of this PDF file must comply with the IEICE Provisions on Copyright.**

**The author(s) can distribute this PDF file for research and educational (nonprofit) purposes only.**

**Distribution by anyone other than the author(s) is prohibited.**

**A PUBLICATION OF THE COMMUNICATIONS SOCIETY**



The Institute of Electronics, Information and Communication Engineers  
Kikai-Shinko-Kaikan Bldg., 5-8, Shibakoen 3chome, Minato-ku, TOKYO, 105-0011 JAPAN

# RSSI-Based Living-Body Radar Using Single RF Front-End and Tunable Parasitic Antennas

Katsumi SASAKI<sup>†a)</sup>, Student Member, Naoki HONMA<sup>†</sup>, Member, Takeshi NAKAYAMA<sup>††</sup>, and Shoichi IIZUKA<sup>††</sup>, Nonmembers

**SUMMARY** This paper presents the Received-Signal-Strength-Indicator (RSSI) based living-body radar, which uses only a single RF front-end and a few parasitic antennas. This radar measures the RSSI variation at the single active antenna while varying the terminations of the parasitic antennas. The propagation channel is estimated from just the temporal transition of RSSI; our proposal reconstructs the phase information of the signal. In this paper, we aim to estimate the direction of living-body. Experiments are carried out and it is found that most angular errors are within the limit of the angular width of the living-body.

**key words:** DOA estimation, parasitic antenna, RSSI, microwave sensors

## 1. Introduction

Microwave sensors for living-body detection have been well studied [1]–[6]. When the microwave is irradiated on the living-body, the amplitude and phase of the reflected waves are changed due to the movement of the living-body surface. To the best of our knowledge, the benefits of microwave sensing are: 1) the unawareness living-body sensing, 2) privacy protection.

Many attempts to use array antennas for living-body sensing have been presented [3]–[6], and they fall into two groups. The aim of the first group [3], [4], is sensitivity enhancement of the existence detection of living-bodies. Combining the signals received at all antenna elements yields a high detection rate. The second group aims to find the direction or location of the living-bodies [5], [7]. For detecting the location of a living-body, a key advance was the MIMO radar technique [8]. Even though the second group well works in detecting targets, they require expensive hardware, such as synchronized multiple transmitters/receivers, whereas the some of the first group require just phaseless information, i.e. the Received-Signal-Strength-Indicator (RSSI).

A method of estimating a complex MIMO channel created by just a single exciting antenna and multiple parasitic antennas with variable reactance elements has been proposed [9], [10]. These methods estimate the MIMO channel from the single channel response modulated by the parasitic antennas, which is called the load modulation technique. This

scheme yields complex MIMO channel estimation with just a single RF front-end at each side. Moreover, [10] presented a method of restoring phase information from the RSSI of the channel.

By combining these methods, the authors proposed an RSSI-based method for estimating living-body direction using parasitic antennas [11]. In this method, the RSSI of the propagation channel is measured by a simple system consisting of a single receiver and parasitic antennas. The complex propagation channel is estimated from just received RSSI. Living-body direction is estimated by extracting the vital-sign-related component from the time-varying channel. This method significantly simplifies the RF front-end by reducing the number of receivers. Moreover, it does not need phase information of the signal, which allows the use of commercially available receivers, such as Wi-Fi and Bluetooth hardware. Here, there are similar methods such as ‘ESPAR antenna’ [12]. This method uses dipole antennas, and only the DOA estimation of the signal is performed. On the other hand, [11] uses patch antennas and focuses on the estimation of the living-body direction. Moreover, this technique enables to extract only the signal through the living-body, excluding the fixed component such as reflected waves from walls and floors. But in the prior study, the complex channel was measured in advance, and load modulation was performed numerically.

This paper experimentally evaluates the living-body radar proposal, and so estimates target direction using only RSSI and a single RF front-end with parasitic antennas. In this paper, load modulation is performed by connecting variable impedances to the parasitic antennas, and measuring the RSSI with a single RF front-end. In the rest of the paper, the proposed method of estimating living-body direction is reviewed and detailed. After that, the results of the experiment are presented to confirm that the proposed method is effective in estimating living-body direction.

## 2. Proposed Method of Estimating Living-Body Direction

### 2.1 Antenna Model and Propagation Environment Model

Figure 1 shows antenna system model in the proposed method. This system is composed of a transmitting antenna and an active receiving antenna, and  $M$ -element parasitic antennas terminated by load impedances. In the following,

Manuscript received February 15, 2017.

Manuscript revised June 15, 2017.

Manuscript publicized August 22, 2017.

<sup>†</sup>The authors are with the graduate school of Engineering, Iwate University, Morioka-shi, 020-8551 Japan.

<sup>††</sup>The authors are with Panasonic Corporation, Kadoma-shi, 571-8501 Japan.

a) E-mail: t2316021@iwate-u.ac.jp

DOI: 10.1587/transcom.20171SP0022

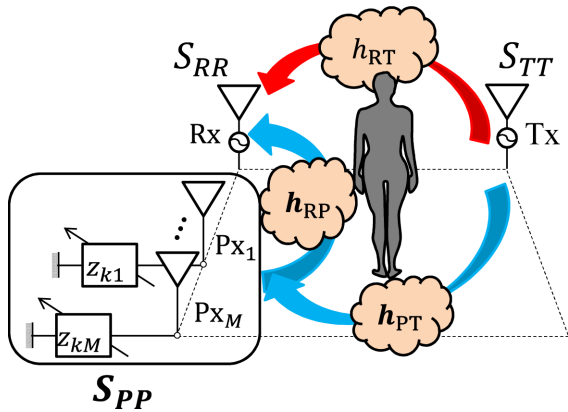


Fig. 1 Antenna system model.

subscripts  $T$ ,  $R$ , and  $P$ , refer to the transmitting (Tx), receiving (Rx), and parasitic (Px) ports, respectively. In this antenna system, the S-parameters are expressed as

$$\mathbf{S} = \begin{bmatrix} S_{TT} & h_{TR} & \mathbf{h}_{TP} \\ h_{RT} & S_{RR} & \mathbf{h}_{RP} \\ \mathbf{h}_{PT} & \mathbf{h}_{PR} & S_{PP} \end{bmatrix} \quad (1)$$

where,  $h_{RT}$  represents the channel response from Tx to Rx antennas, for example. Note that,  $h_{RT}$  cannot be directly observed since the signal observed at Rx also contains scattered paths from the parasitic elements and they cannot be separated normally.  $h_{PT}$  represents the channel response from Tx to Px antennas, and this is not directly observable, too.  $h_{RP}$  are S-parameters that represent coupling between Rx and Px antennas. Since  $\mathbf{S}$  is a symmetric matrix, the relations,  $h_{TR} = h_{RT}$ ,  $\mathbf{h}_{TP} = \mathbf{h}_{PT}^T$ , and  $\mathbf{h}_{PR} = \mathbf{h}_{RP}^T$  are satisfied, where  $\mathbf{h}_{TP}$  and  $\mathbf{h}_{RP}$  are column vectors, and  $\mathbf{h}_{PT}$  and  $\mathbf{h}_{PR}$  are row vector.  $S_{TT}$ ,  $S_{RR}$ , and  $S_{PP}$  represent the S-parameters of Tx, Rx and Px antennas, respectively. Among the mentioned elements,  $h_{TR} = h_{RT}$  and  $\mathbf{h}_{TP} = \mathbf{h}_{PT}^T$  correspond to the channels between the transmitter and receiver sides, which is unknown and may vary due to the antenna arrangement and the environment. On the other hand,  $S_{TT}$ ,  $S_{RR}$ ,  $S_{PP}$ , and  $\mathbf{h}_{PR} = \mathbf{h}_{RP}^T$  represent the characteristics of the antennas that are normally constant and they can be measured when the antennas are produced.

When the parasitic elements are terminated by load impedance elements, whose termination condition is defined as  $\mathbf{\Gamma}$ , the signal strength is given by

$$|y| = |h_{RT} + \mathbf{h}_{RP}(\mathbf{\Gamma}^{-1} - S_{PP})^{-1}\mathbf{h}_{PT}| |s| \quad (2)$$

where  $s$  represents the signal transmitted from Tx antenna, and the termination condition is

$$\mathbf{\Gamma} = \text{diag}(\gamma_1, \dots, \gamma_M) \quad (3)$$

where  $\gamma_m$  is the reflection coefficient of the terminating load at the  $m$ -th Px antenna. When  $z_0$  is the reference impedance and  $z_m$  is the load impedance at the  $m$ -th Px antenna,  $\gamma_m$  is calculated as

$$\gamma_m = \frac{z_m - z_0}{z_m + z_0} \quad (4)$$

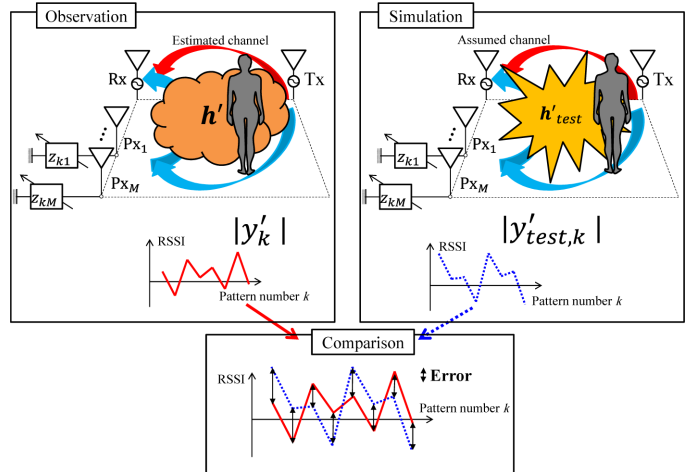


Fig. 2 Concept of the evaluation function.

## 2.2 Method of Estimating the Propagation Channel

In this study, the complex single-input multiple-output (SIMO) channel vector,  $[h_{RT}, \mathbf{h}_{RP}^T]^T$ , is estimated from the RSSI response of the single RF front-end while the load impedances at the Pxs are varied. Figure 2 depicts the concept of the evaluation function, which is one of the key ideas in this method. At first, the temporal transition is observed during the period corresponding to the cycle with  $K$ -set terminations. The  $K$ -sets of the load impedances at the Px array are defined as

$$\mathbf{Z} = \begin{bmatrix} \mathbf{Z}_1 \\ \vdots \\ \mathbf{Z}_K \end{bmatrix} = \begin{bmatrix} z_{11} & \dots & z_{1M} \\ \vdots & \ddots & \vdots \\ z_{K1} & \dots & z_{KM} \end{bmatrix} \quad (5)$$

where  $K$  represents the number of variable impedance patterns.  $\mathbf{Z}_k$  represents a row vector expressed as  $[z_{k1} \dots z_{km} \dots z_{kM}]$ , where  $z_{km}$  represents the load impedance at the  $m$ -th Px antenna in the case of the  $k$ -th termination pattern. That is, in the case of the  $k$ -pattern, the  $M$ -element Px antennas are simultaneously terminated by the impedance set represented by  $\mathbf{Z}_k$ .

In this study, the termination conditions are changed and the resulting signals are observed, where  $K$  patterns of the conditions are given within a sufficiently short period that must be shorter than the cycle of the vital-life sign. The cycle of  $K$  times observation described above is repeated  $L$  times to observe the temporal variation of the channel due to the vital sign. Here, the measurement period of  $L$  time cycle needs to be sufficiently long, and can be comparable to the cycle of the vital-life sign. In measuring the  $l$ -th ( $1 \leq l \leq L$ ) snapshot, the received signal strength in the  $k$ -th ( $1 \leq k \leq K$ ) termination pattern is defined as  $|y_k^{(l)}|$ .

Multi-path environments contain unnecessary waves such as the direct wave between the Tx/Rx antennas and waves reflected from the wall. They need to be eliminated to estimate the living-body direction correctly. Therefore,

the mean signal strength over a certain period is subtracted from the observed signal strength because the mean value corresponds to the constant channel component, which is not thought to contain the vital sign. At the  $l$ -th measurement, the signal strength through the living-body, excluding the fixed component, is expressed as

$$|y_k^{(l)}| = |y_k^{(l)}| - \frac{1}{L} \sum_{l=1}^L |y_k^{(l)}| \quad (6)$$

Now, let us explain the simulation part depicted in Fig. 2. In the first step, the arbitrary complex SIMO channel vector is assumed to be,

$$\mathbf{h}'_{test}{}^{(l)} = \begin{bmatrix} h'_{test,R} \\ h'_{test,P1} \\ \vdots \\ h'_{test,PM} \end{bmatrix} \quad (7)$$

where  $h'_{test,R}$  represents the channel between Tx and Rx antennas, and  $h'_{test,Pm}$  represents the channel between Tx and Px antennas in the  $m$ -th element. Note that the assumed channel does not necessarily agree with the true channel at this moment. This assumed channel is translated into an RSSI transition using the expression of,

$$|y'_{test,k}| = \left| \mathbf{h}'_{test,R} + \mathbf{h}_{RP} (\mathbf{\Gamma}_k^{-1} - \mathbf{S}_{PP})^{-1} \begin{bmatrix} h'_{test,P1} \\ \vdots \\ h'_{test,PM} \end{bmatrix} \right| |s|, \quad (8)$$

where the termination condition in the  $k$ -th termination pattern is

$$\mathbf{\Gamma}_k = \text{diag}(\gamma_{k1}, \dots, \gamma_{kM}). \quad (9)$$

$\gamma_{km}$  represents the reflection coefficient of the terminating load of the Px antenna in the  $m$ -th element, as expressed in (4)

The simulated RSSI transition calculated by (8) is compared with the actually observed one by using the evaluation function defined as,

$$e^l = \frac{1}{K} \sum_{k=1}^K \left| |y_k^{(l)}| - |y'_{test,k}{}^{(l)}| \right|, \quad (10)$$

which is the square-mean of the value differences over  $K$ -set trials.

After that, the initially assumed channel is iteratively optimized so as to make the signal responses estimated from it fit the observed responses, i.e. this is the minimization problem detailed in (10). In this study, the steepest descent method is used to minimize  $e^l$ . In the steepest descent method, the initial value, i.e. the first assumed channel, determines the convergence and accuracy of the solution. Hence, a realistic channel vector needs to be chosen as the initial value. Since the aim of this study is identification of target

direction, the incoming wave will arrive from a certain direction. Therefore, multiple steering vectors are initially used, where their directions are determined with uniform directional difference to cover the designated extent of detection. We use the universal steering vector [13] defined as,

$$\mathbf{h}'_{test}{}^{(l)}(\theta_S) = X \begin{bmatrix} D_R(\theta_S) \\ D_{P1}(\theta_S) \\ \vdots \\ D_{PM}(\theta_S) \end{bmatrix} \quad (11)$$

where  $X$  is the arbitrary value determining the amplitude of the steering vector, and  $D_R$  and  $D_{Pm}$  are the complex directivities of Rx and  $m$ -th Px antennas, respectively. The steepest gradient algorithm is applied to the multiple steering vectors with various directions,  $\theta_S$ , and we chose the best solution, i.e., the one with the smallest error. The target direction is calculated from the estimated channel by using the MUltiple Signal Classification (MUSIC) method [14]. Here, since the relationship between ‘the antenna-target distance’ and ‘the amplitude of the received signal’ is complicated due to the multi-path fading [15], it is difficult to estimate the antenna-target distance accurately.

### 3. Experimental Conditions and Environment

To verify the performance of the proposed method in an actual environment, an experiment was conducted. Table 1 shows the measurement conditions. A varactor diode was connected to Px antennas, and its terminal condition was controlled by the bias voltage. Antenna height  $H$  was 1.05 m, and the distance between antennas and target was 1.5 and 3.0 m. The number of termination sets was  $K = 9$ , and channel snapshot frequency was 100 Hz, which corresponds to the switching time of the termination set, and the total observation period was 9.0 s. This means the SIMO channel vectors are estimated every 0.09 s, and the total number of channel estimations in the complete observation period was  $L = 100$ . Figure 3 shows the measurement environment, and Fig. 4 shows a measurement scene. The target stood straight upright at the position of  $-40^\circ \leq \theta_R \leq 40^\circ$  with respect to the broadside direction of the array.

Figure 5 shows the measurement system. The RF signal output from the signal generator was branched through the divider. One signal was sent to the Tx antenna through a variable attenuator and power amplifier so that the transmis-

**Table 1** Measurement condition.

|                                      |                          |
|--------------------------------------|--------------------------|
| Antenna configuration                | 1×1 SISO + 2 Px elements |
| Antenna height $H$ [m]               | 1.05                     |
| Frequency [GHz]                      | 2.47                     |
| Termination sets $K$                 | 9                        |
| Snapshot frequency [Hz]              | 100                      |
| Measurement time [s]                 | 9.0                      |
| Gamma switching time [s]             | 0.01                     |
| Total observation period $L$         | 100                      |
| Antenna-target distance $D_{RT}$ [m] | 1.5, 3.0                 |
| Target position $\theta_R$ [°]       | -40, -30, ..., 40        |

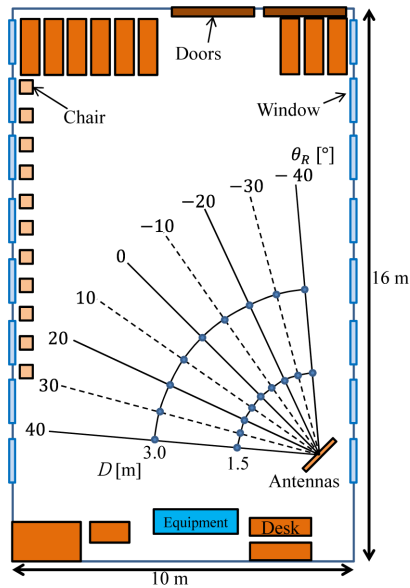


Fig. 3 Measurement environment.

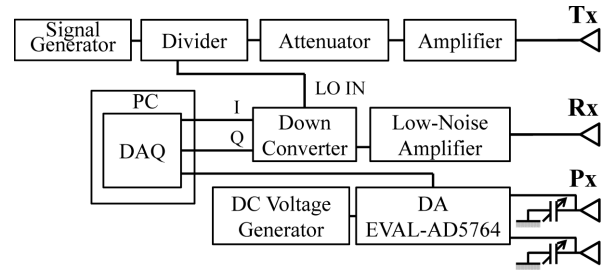


Fig. 5 Measurement system.

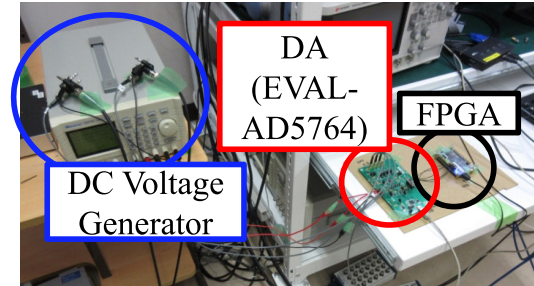


Fig. 6 Load modulator.

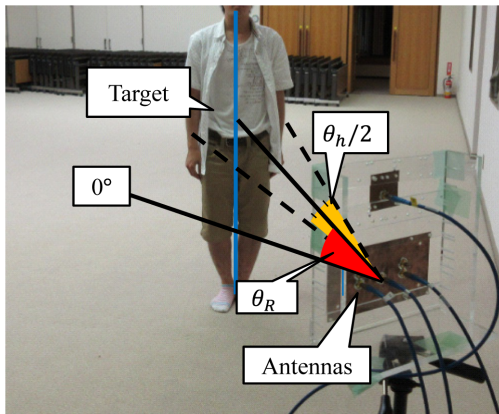


Fig. 4 Measurement scenery.

sion power was set at 10 dBm. Figure 6 shows a photo of the load modulator. The voltage output from the DC (direct current) voltage generator was applied to the bias port of the Px antenna via the DA (Digital to Analog) converter. Here, an FPGA (field-programmable gate array) was used to control the voltage value from the AD converter. In order to synchronize the control signal with the PC, a synchronization signal was sent from the DA converter to the DAQ (Data Acquisition Unit).

Figure 7 shows the Rx and Px antennas used in this experiment. The receiving array consisted of three element antennas, where the center element was the Rx antenna and other two elements were Px antennas. The inter-antenna interval (center-to-center) was about 0.4 wavelengths. In order to enhance mechanical robustness, FR4 substrate was used. Also, in order to achieve an array with high radiation efficiency and wide aperture, an air layer was formed between the patch conductor layer (upper substrate) and the ground layer (lower substrate). The thickness of the air layer

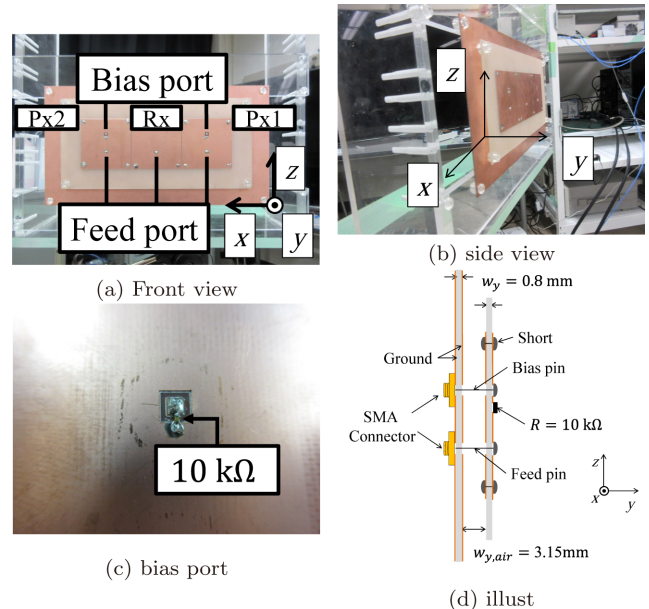


Fig. 7 Rx and Px antennas.

$y_{air}$  was 3.15 mm. SMA connectors were attached to the backside of the lower substrate, i.e., each patch has a single feed port. The Px antenna element was configured with a termination port that connects the varactor diode, and a bias port is provided on the antenna element. Figure 7(c) shows a close-up of the bias port. The DC cable on the backside was connected via a resistance,  $R$ , with value of 10 k $\Omega$ . Therefore, when DC bias is applied, a reverse bias is applied to the varactor diode. Although the resistor and the varactor diode are connected in series, no voltage drop occurs in the resistor because so little DC current flows. Therefore, the DC bias is

applied only to the varactor diode. On the other hand, since the resistance value  $R$  is large, no RF signal flows to the bias port. As described above, the use of the high impedance resistance makes it possible to realize a bias port that does not affect the RF characteristics.

**4. Results**

Figure 8 shows the reflection coefficient of the varactor diode used in this experiment. When the voltage applied to the varactor diode,  $V$ , is changed from 0 V to 20 V, the reflection coefficient draws the trajectory shown in the figure. In this experiment, the voltage value is set so that the phase interval of the reflection coefficients is uniform.  $\Gamma_{Px1}$  and  $\Gamma_{Px2}$  represent the reflection coefficients of the varactor diodes connected to the parasitic antennas, Px1 and Px2, respectively. They should be same theoretically, but slightly different due to manufacturing error.  $\Gamma_{Pxm1}$ ,  $\Gamma_{Pxm2}$ ,  $\Gamma_{Pxm3}$  represent the reflection coefficients for  $V = 0, 7.7$ , and 20 V, respectively. Figure 9 shows the directivity of the Rx antenna when the Px antennas are terminated. Here, we compared the directivity of the termination processing by numerical analysis after directivity measurement and the directivity measured by actually connecting the varactor diode to the Px antennas. Since each Px antenna element is terminated by varactor diodes of three reflection coefficients, a total of 9 directivity patterns were observed. From the figure, it can be seen that the form of the directivity changes with each termination condition.

Figure 10 shows the signal strength variation over the observation time. Here, Fig. 10(a) shows the intensity variation over all measurements. In this figure, the variation of the respiration component is seen at a period of about 3 s. Also, Fig. 10(b) shows the close-up of (a) in the range of 3.9 s to 4.1 s. As indicated in this figure, the unit measurement period is defined as the period corresponding to the cycle of the  $K$  sets of the terminations, where  $K = 9$  in this experiment. It can be seen that the signal strength changes in accordance with the impedance pattern number,

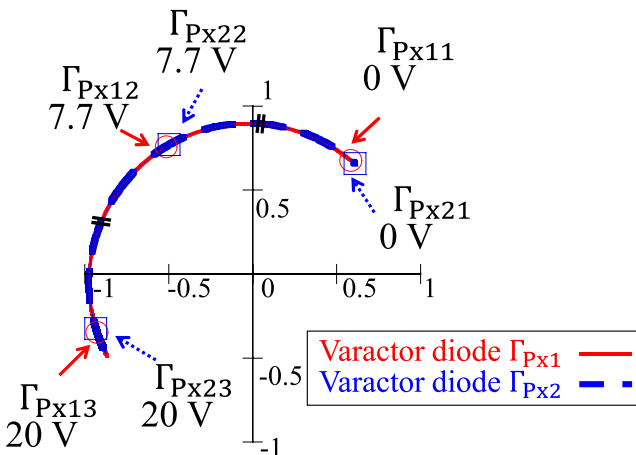


**Fig. 8** Reflection coefficient of varactor diode.

$k$ , and a similar waveform appears periodically at every unit measurement period, which is set to 0.09 s.

Figure 11 shows how the steepest descent method makes the amplitude error of the channel converge by performing optimization so that the evaluation function of (10) becomes minimum. The horizontal axis represents the number of trials of the steepest descent method, and the vertical represents the amplitude error defined by (10). Here, the number of iterations of the steepest descent method was set to 50. It can be seen the amplitude error of the channel decreased step by step. Also, it is found that the convergence speed and

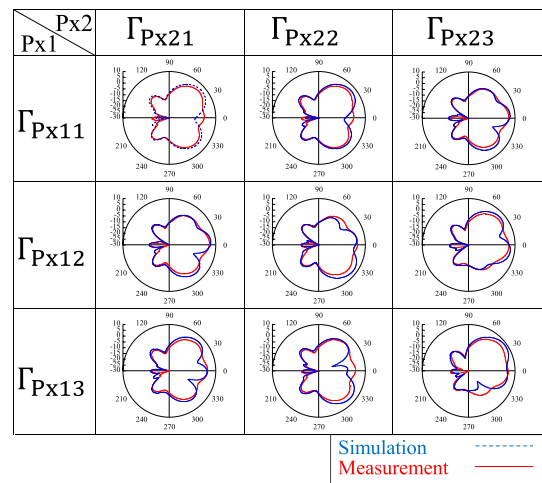
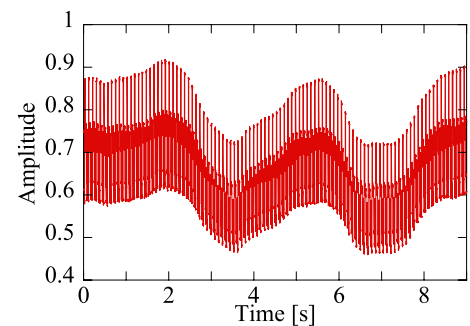
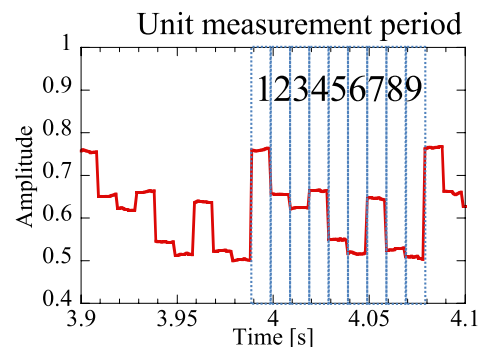


**Fig. 9** Directivity.



(a) all measurement times



(b) 3.9 s ~ 4.1 s

**Fig. 10** Observed signal strength.

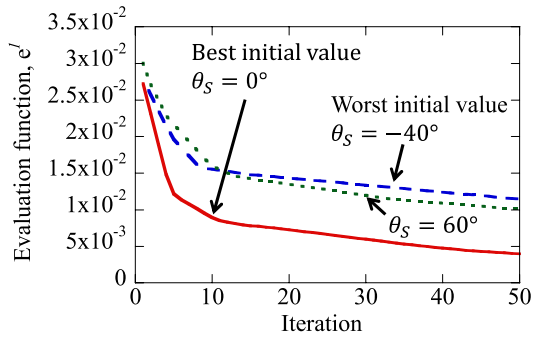


Fig. 11 Steepest descent.

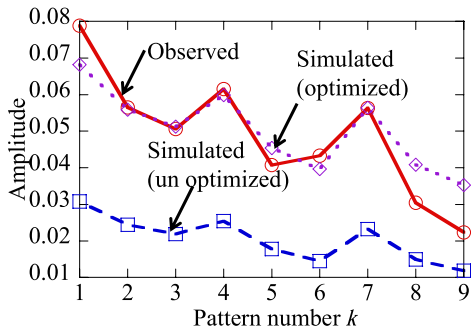
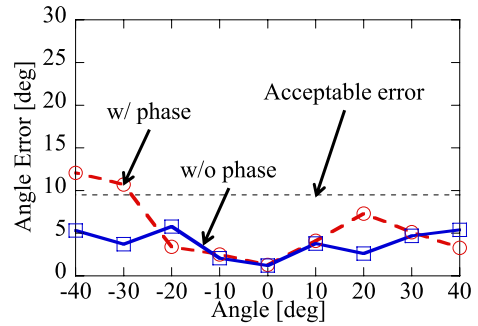


Fig. 12 RSSI comparison.

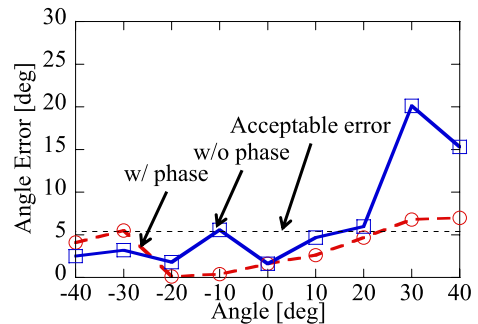
accuracy significantly depend on the initial values, and the error with the best initial channel converges into 2.89 times smaller than that with the worst one does, where the best initial value,  $\theta_s = 0^\circ$ , just corresponds to the exact direction of the target.

Figure 12 compares the signal strength transitions of the actual observation and simulations before and after optimization. ‘Observed’ means the actually observed signal strength through the living-body. This value is expressed by (6) in Sect. 2.2. On the other hand, the dotted and dashed lines are the values calculated by simulation. As a first step of the channel estimation, our method assumes a complex channel as shown in (7). The dashed line represents the response calculated by using (8) with the initially assumed channel, and this is indicated as ‘Simulated (un optimized).’ By substituting the optimized complex channels into that in (8), the dotted line, ‘Simulated (optimized),’ is calculated. As described in Sect. 2.2, the mean signal strength over a certain period is subtracted from the observed signal strength. From this result, it can be seen the optimization well predicts the signal strength transition, that is, the complex SIMO channel is well estimated.

In this study, the evaluation criteria for angular estimation are based on the angular width of the human body. If the estimated angular error is less than one half the angular width of the human body, it is judged that the living-body direction was accurately estimated. For the human body width of 0.50 m and the distances between the antennas and target of 1.5 m and 3.0 m, the acceptable error is  $9.5^\circ$  and  $4.8^\circ$ , respectively.



(a)  $D = 1.5$  m



(b)  $D = 3.0$  m

Fig. 13 Center value of the angular errors.

To evaluate the accuracy of the proposed method, we conducted the DOA estimation with full RF front-ends, i.e. all antennas individually have synchronized receivers, where all other conditions, such as array configurations, are identical. Figure 13 shows the median value of the angular errors versus the target direction. Here, the estimation was performed 20 times at each target direction. In this figure, good agreement between the result with phase and without phase can be confirmed. Also focusing on the angular error for  $\theta_R < 30^\circ$ , estimation of direction was possible within the acceptable angular error. Figure 14 shows the CDF (Cumulative-Distribution-Function) of the angular error. Focusing of 50% values, when the distance between the antennas and target was 1.5 m and 3.0 m, the angular error was  $3.9^\circ$  and  $4.3^\circ$ , respectively. Therefore, the angular error was less than the acceptable error. From the above, it was confirmed that the proposed estimation method is effective when varactor diodes actually terminate the Px antennas.

### 5. Conclusion

This paper has presented experiments that validate the living-body direction estimation method that relies on just the RSSI of a single RF front-end antenna system with several parasitic antennas. The experiments were conducted using three-microstrip-antenna arrays terminated by varactor diodes. It was found that the proposed method successfully identified the direction of the target even though the environment was

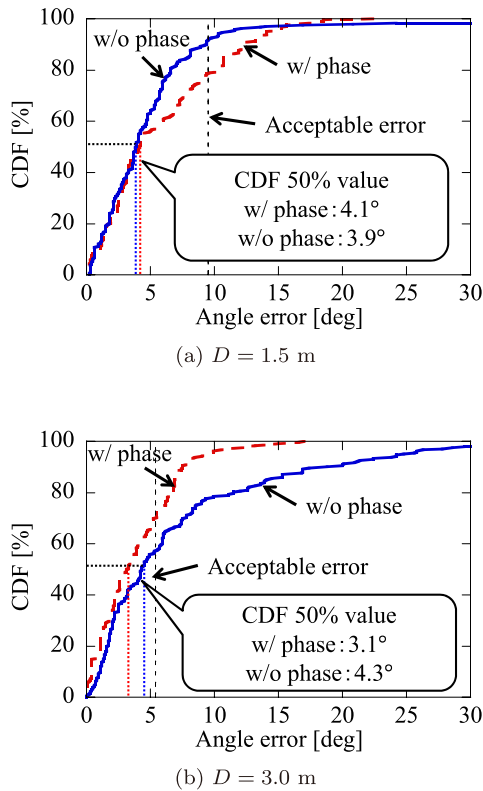


Fig. 14 CDF of the angular errors.

multipath, and the median angular error was  $3.9^\circ$  and  $4.3^\circ$  when the distance between the antennas and target was 1.5 m and 3.0 m, respectively. This means the angular error is less than the angular width of the human body. From the above, we confirmed that the proposed method well estimates the direction of the living-body from just the amplitude information captured by a single RF front-end. These results proved that the proposed method well estimates the living-body direction even with simple devices. In our future work, the estimation of the location and motion will be investigated by extending the proposed method.

## References

- [1] M. Nishi, S. Takahashi, and T. Yoshida, "Indoor human detection systems using VHF-FM and UHF-TV broadcasting waves," Proc. 2006 IEEE Int. Symp. Personal Indoor Mobile Radio Commun. (PIMRC), Sept. 2006.
- [2] Y. Okugawa, Y. Akiyama, H. Yamane, and K. Tajima, "Study on an intrusion detecting method using TV broadcasting waves," Proc. 2007 Int. Symp. Antennas and Propagat. (ISAP), POS 1-25, pp.955–958, Nov. 2007.
- [3] S. Ikeda, H. Tsuji, and T. Ohtsuki, "Indoor event detection with signal subspace spanned by eigenvector for home or office security," IEICE Trans. Commun., vol.E92-B, no.7, pp.2406–2412, July 2009.
- [4] K. Ushiki, K. Nishimori, N. Honma, and H. Makino, "Intruder detection performance of SIMO and MIMO sensors with same number of channel responses," IEICE Trans. Commun., vol.E96-B, no.10, pp.2499–2505, Oct. 2013.
- [5] Y.J. An, B.J. Jang, and J.G. Yook, "Detection of human vital signs and estimation of direction of arrival using multiple Doppler radars," J. Korean Institute of Electromagnetic Engineering and Science, vol.10, no.4, pp 250–255, Dec. 2010.
- [6] K. Konno, M. Nango, N. Honma, K. Nishimori, N. Takemura, and T. Mitsui, "Experimental evaluation of estimating living-body direction using array antenna for multipath environment," IEEE Antennas Wireless Propag. Lett., vol.13, pp.718–721, April 2014.
- [7] K. Konno, N. Honma, D. Sasakawa, K. Nishimori, N. Takemura, and T. Mitsui, "Estimating living-body location using bistatic MIMO radar in multi-path environment," IEICE Trans. Commun., vol.E98-B, no.11, pp.2314–2321, Nov. 2015.
- [8] J. Li and P. Stoica, MIMO Radar Signal Processing, A John Wiley Sons, 2009.
- [9] N. Honma, "Method of MIMO channel estimation between parasitic antenna arrays," IEEE Trans. Antennas Propagat., vol.61, no.5, pp.2792–2800, May 2013.
- [10] D. Pinchera and M.D. Migliore, "A phaseless parasitic MIMO-channel sounder," Proc. IEEE Antennas and Propagation Society Int. Symp., 2008.
- [11] K. Sasaki, N. Honma, T. Nakayama and S. Iizuka, "RSSI-based estimation method of living-body direction using parasitic antennas," 2016 Int. Symp. Antennas and Propagat. (ISAP), pp.924–925, Oct. 2016.
- [12] E. Taillefer, A. Hirata, and T. Ohira, "Direction-of-arrival estimation using radiation power pattern with an ESPAR antenna," IEEE Trans. Antennas Propag., vol.53, no.2, pp.678–684, Feb. 2005.
- [13] Q. Yuan, Q. Chen, and K. Sawaya, "Accurate DOA estimation using array antenna with arbitrary geometry," IEEE Trans. Antennas Propagat., vol.53, no.4, pp.1352–1357, April 2005.
- [14] R.O. Schmidt, "Multiple emitter location and signal parameter estimation," IEEE Trans. Antennas Propagat., vol.AP-34, no.3, pp.276–280, 1986.
- [15] P.K. Sahu, E.H.-K. Wu, and J. Sahoo, "DuRT: Dual RSSI trend based localization for wireless sensor networks," IEEE Sensors J., vol.13, no.8, pp.3115–3123, Aug. 2013.



**Katsumi Sasaki** received the B.E. degree in electrical and electronic engineering from Iwate University, Morioka, Japan in 2016. He is currently in the master program in Iwate University. His current research interest is RSSI-based living-body radar using parasitic antennas.



**Naoki Honma** received the B.E., M.E., and Ph.D. degrees in electrical engineering from Tohoku University, Sendai, Japan in 1996, 1998, and 2005, respectively. In 1998, he joined the NTT Radio Communication Systems Laboratories, Nippon Telegraph and Telephone Corporation (NTT), in Japan. He is now working for Iwate University. He received the Young Engineers Award from the IEICE of Japan in 2003, the APMC Best Paper Award in 2003, the Best Paper Award of IEICE Communication Society in 2006, and 2014 Asia-Pacific Microwave Conference Prize in 2014, respectively. His current research interest is MIMO system and its applications. He is a member of IEEE.



**Takeshi Nakayama** received the B.E., M.E. degrees in Department of Opt-electronic & Mechanical Engineering, Faculty of Engineering from Shizuoka University, Shizuoka, Japan in 1994, 1996, respectively. In 1996, he joined the Multimedia Development Center, Matsushita Electric Industrial Co., Ltd. (Panasonic Corporation), in Japan. He is now working for Panasonic Corporation. His current research interest is MIMO system and its applications.



**Shoichi Iizuka** received the B.E. and M.E. degrees in information science and technology from Osaka University, Osaka, Japan in 2013 and 2015, respectively. He joined Appliances Company, Panasonic Corporation in 2015. His current research interest is living-body radar system and its applications. He is a member of Information Processing Society of Japan.